J Nanostruct 16(3): 3718-3730, Summer 2026

RESEARCH PAPER

Nano-Resveratrol Preserves Keratinocyte Physiological Homeostasis Against UVA-Induced Oxidative Disruption

Ahmed R. Albuhaydar

College of Pharmacy, University of Al-Qadisiyah, Iraq

ARTICLE INFO

Article History:
Received 13 April 2026
Accepted 26 June 2026
Published 01 July 2026

Keywords:
Calcium homeostasis
Inflammation
Keratinocyte physiology
Mitochondrial function
PLGA nanoparticles

ABSTRACT

Maintaining cellular homeostasis in epidermal keratinocytes — including membrane integrity, mitochondrial bioenergetics, intracellular Ca^{2+} regulation, redox balance, and inflammatory tone is essential for skin function and is highly vulnerable to UVA-driven oxidative disruption. Resveratrol (Res), a natural stilbenoid antioxidant, has shown promising photoprotective effects, although its therapeutic potential is constrained by poor aqueous solubility and rapid photodegradation. In the present work, we examined whether pretreatment with PLGA-encapsulated Res nanoparticles (Res-NPs) is able to preserve a broad set of physiological functions in cultured human keratinocytes (HaCaT) following UVA irradiation (10 J/cm²). Compared with the free compound at equivalent concentration (50 μM), Res-NPs markedly reduced UVA-induced lactate dehydrogenase (LDH) leakage (~38% - ~9% of total) and preserved the mitochondrial membrane potential, with the JC-1 red/green ratio held at about 89% of basal values. Intracellular ATP was maintained at 88% of control, while the typical UVA-driven Ca^{2+} overload was substantially attenuated (held below 1.2-fold of basal vs. 2.8-fold for UVA alone). Redox homeostasis was preserved, with the GSH/GSSG ratio close to physiological values. Pro-inflammatory cytokine secretion (IL-6, IL-8, TNF-α) was suppressed by ~70–80%. Furthermore, qPCR analysis showed that Res-NPs largely restored the expression of late differentiation markers (filaggrin, involucrin, loricrin), and the scratch-wound assay revealed near-normal migratory capacity (≈89% closure at 48h). Taken together, these results support nanoencapsulation as an effective strategy for safeguarding the integrated physiological functions of keratinocytes under UVA stress.

How to cite this article
R. Albuhaydar A. Nano-Resveratrol Preserves Keratinocyte Physiological Homeostasis Against UVA-Induced Oxidative Disruption, 2026; 16(3):3718-3730. DOI: 10.22052/JNS.2026.03.060

INTRODUCTION

Skin keratinocytes constitute the principal cellular component of the epidermis and are continuously exposed to environmental stressors, particularly solar ultraviolet (UV) radiation [1,2]. About 95% of UV rays reaching the skin surface are UVA wavelengths (320–400 nm), which penetrate deeply into the dermis and cause cellular damage by generating ROS [3]. ROS affect plasma membrane integrity, mitochondrial energetics, intracellular calcium signalling, redox balance, and inflammatory tone in addition to cytotoxicity [4–6]. Analogous ROS-driven pathology has also been documented in non-cutaneous tissues, including

* *Corresponding Author Email: ahmed.riyadh@qu.edu.iq*

iron overload syndromes (β-thalassemia) and their ophthalmologic complications [7,8]. Cellular homeostasis declines, causing photoaging, barrier failure, and skin diseases such carcinogenesis [9]. Such susceptibility is amplified in vulnerable groups, particularly pediatric populations affected by metabolic disorders and related health conditions [10–12].

Under such stress, plant-derived polyphenols are promising keratinocyte support agents [13]. Beyond polyphenols, diverse heterocyclic scaffolds and small-molecule libraries have likewise attracted interest as bioactive agents [14,15]. Resveratrol (3,4',5-trihydroxystilbene), a compound abundant in the skin of red grapes, peanuts and berries, is known to have the potential to scavenge ROS, activate Nrf2/ARE pathway and suppress NF-κB signalling [16-18]. The low water solubility, rapid metabolism and photochemical stability lead to low bioavailability and skin uptake, which makes it inappropriate for topical treatment [19,20]. PLGA nanoencapsulation has been shown to overcome these limitations, increasing the stability of the medicine and enhancing the intracellular delivery [21-23]. Complementary nanomaterial classes including activated nano-carbon platforms and silver phosphate–chitosan nanocomposites further illustrate the breadth of nanotechnology applications in biomedical and environmental fields [24,25].

However, most of the investigations have focused on standard photoprotective end points, such as viability loss, lipid peroxidation, and apoptosis, and less on how the nanoencapsulation of resveratrol modulates keratinocyte physiological homeostasis. The present work fills this gap. PLGA-encapsulated Res-nanoparticles (Res-NPs), prepared and characterized in our previous study [26], were applied to cultured HaCaT keratinocytes prior to UVA exposure (10 J/cm²), and a broad panel of physiologically relevant readouts-membrane integrity, mitochondrial membrane potential, ATP content, intracellular Ca^{2+}, GSH/GSSG ratio, pro-inflammatory cytokines, late differentiation markers, and migratory capacity was systematically evaluated.

MATERIALS AND METHODS

Chemicals and Reagents

trans-Resveratrol (≥98%), poly(lactic-co-glycolic acid) (PLGA, 50:50, Mw 30–60 kDa), poloxamer 188, JC-1, Fluo-4 AM, dimethyl sulfoxide (DMSO), and most other chemicals were purchased from Sigma-Aldrich (St. Louis, MO, USA). LDH cytotoxicity assay kit, ATP determination kit, and the GSH/GSSG-Glo assay kit were obtained from Promega (Madison, WI, USA). Human IL-6, IL-8 and TNF-α ELISA kits were sourced from R&D Systems (Minneapolis, MN, USA). DMEM, fetal bovine serum (FBS), and antibiotic mixture were supplied by Gibco (Thermo Fisher Scientific, USA). Ultrapure water (Milli-Q, Millipore, France) was used throughout the work, and all other reagents were of analytical grade.

Preparation and Characterization of Res-NPs

Resveratrol-loaded PLGA nanoparticles (Res-NPs) were prepared by a modified nanoprecipitation method, exactly as described in our previous study [26]. Briefly, 50 mg of PLGA and 10 mg of resveratrol were dissolved in 5 mL of acetone and injected slowly into a 25 mL aqueous phase containing 0.5% (w/v) poloxamer 188 under continuous magnetic stirring. After complete evaporation of the organic solvent, nanoparticles were collected by ultracentrifugation (15,000 ×g, 30 min, 4 °C), washed twice with ultrapure water, and finally lyophilized using 5% (w/v) trehalose as cryoprotectant. The optimized formulation showed a hydrodynamic diameter of 152.4 ± 6.8 nm, a polydispersity index of 0.182, a zeta potential of −28.3 mV, and an encapsulation efficiency of 84.7 ± 2.1% [26]. Blank nanoparticles (B-NPs) were prepared in an identical manner without the drug and used as carrier controls.

Scanning Electron Microscopy (SEM)

The surface shape and particle size of lyophilised Res-NPs were observed by using the field emission scanning electron microscopy (FE-SEM, FEI Inspect F50, Thermo Fisher Scientific, USA) [27]. A little amount of the nanoparticle powder was re-suspended in ultrapure water (0.1 mg/mL) and a 10 µL drop of the suspension was placed on a clean silicon wafer and air-dried at room temperature in a desiccator. The dried specimen was attached to an aluminium stub using double-sided carbon tape and then coated with a thin coating of gold (8 nm) under vacuum (Quorum Q150R ES sputter coater) to assure conductivity. Micrographs were taken at high vacuum, accelerating voltage of 15 kV and working distance of 9–11 mm at magnification of 20,000 to 80,000. Particle diameters were quantified from the digital micrographs using

ImageJ software (NIH, USA), measuring at least 150 individual particles per sample, and the resulting size distribution was compared with the hydrodynamic diameter obtained by dynamic light scattering.

X-Ray Diffraction (XRD)

The crystalline state of resveratrol within the polymeric matrix was investigated by powder X-ray diffraction (XRD) on a Bruker D8 Advance diffractometer (Bruker AXS, Germany) equipped with a Cu-Kα radiation source (λ = 1.5406 Å) operating at 40 kV and 40 mA [28]. Lyophilized samples of free resveratrol, blank PLGA nanoparticles (B-NPs) and Res-NPs were gently ground in an agate mortar and packed into a low-background sample holder. Diffraction patterns were recorded at room temperature over a 2θ range of 5°–40°, with a step size of 0.02° and a scan rate of 2°/min. The disappearance or marked attenuation of the sharp Bragg reflections characteristic of crystalline resveratrol in the Res-NPs pattern, together with the appearance of a broad amorphous halo from the PLGA matrix, was taken as direct evidence of molecular dispersion of the drug within the nanoparticles and of successful nanoscale encapsulation.

Cell Culture and UVA Irradiation

HaCaT human keratinocytes (ATCC, USA) were cultured in DMEM supplemented with 10% FBS and 1% penicillin–streptomycin solution at 37 °C in a humidified atmosphere of 5% CO_2. For investigations, cells were seeded in 96- or 6-well plates and pre-incubated with Free-Res, B-NPs or Res-NPs (50 µM resveratrol equivalent) for 4 h. Just before irradiation, the medium was changed with PBS and cells were subjected to UVA radiation at 10 J/cm² (Vilber Lourmat UVA lamp, 365 nm, 5 mW/cm²) [29]. Non-irradiated controls were kept under the same conditions, but wrapped in aluminium foil. After irradiation, cells were returned to fresh complete medium and incubated for 24 h prior to analysis (or as specified for individual assays).

Lactate Dehydrogenase (LDH) Leakage Assay

Plasma membrane integrity was assessed by measuring LDH activity released into the culture supernatant 24 h post-irradiation, using a commercial cytotoxicity kit (Promega) according to the manufacturer's instructions [30]. LDH activity was quantified by measuring absorbance at 492 nm. Data are reported as a percentage of the maximum LDH release obtained from cells lysed with 1% Triton X-100 (taken as 100%).

Mitochondrial Membrane Potential (JC-1)

The mitochondrial membrane potential (ΔΨm) was assessed using the cationic dye JC-1 [31]. After UVA exposure, HaCaT cells were incubated with 5 µM JC-1 in serum-free DMEM for 20 min at 37 °C in the dark. Cells were then washed twice with PBS, and fluorescence was recorded at λex/em = 514/590 nm (red, J-aggregate, indicative of polarized mitochondria) and 488/530 nm (green, monomer, indicative of depolarized mitochondria) using a fluorescence plate reader (BioTek Synergy HT, USA). Results are expressed as the red-to-green fluorescence ratio, normalized to non-irradiated controls.

Intracellular ATP Quantification

Intracellular ATP content was quantified using a luciferase-based ATP determination kit (Promega), as previously described [32]. Briefly, lysates from approximately 5×10^5 cells were prepared in lysis buffer, and luminescence was recorded immediately after addition of the luciferin–luciferase reagent. ATP concentrations were calculated from a standard curve and normalized to total protein content measured by the BCA assay. Results are expressed as a percentage of the non-irradiated control.

Intracellular Calcium Imaging

Free intracellular Ca^{2+} was monitored using the fluorescent indicator Fluo-4 AM [33]. Cells were loaded with 4 µM Fluo-4 AM in HBSS for 30 min at 37 °C in the dark, then washed and equilibrated for an additional 15 min. Fluorescence (λex/em = 488/525 nm) was recorded immediately after UVA irradiation (taken as t = 0) and at 15-min intervals thereafter for 1 h. Results are expressed as the fold change in mean fluorescence intensity (MFI) relative to the non-irradiated control measured at the corresponding time point.

GSH/GSSG Ratio

Intracellular reduced (GSH) and oxidized (GSSG) glutathione levels were quantified using the GSH/GSSG-Glo assay kit (Promega), following the manufacturer's instructions. Data are reported as the GSH/GSSG molar ratio, which is widely accepted as a sensitive index of intracellular redox

state.

Pro-inflammatory Cytokine Quantification (ELISA)

The release of IL-6, IL-8 and TNF-α into the culture medium was quantified using commercial ELISA kits (R&D Systems, USA), following the manufacturer's protocols. Cell culture supernatants were collected 24 h post-irradiation and stored at −80 °C until assayed. All measurements were performed in duplicate, and concentrations were calculated from a four-parameter logistic standard curve.

Quantitative Real-Time PCR (qPCR)

Total RNA was isolated from HaCaT cells 24 h after UVA exposure using TRIzol reagent and reverse-transcribed with a high-capacity cDNA synthesis kit (Applied Biosystems, USA). qPCR was performed with SYBR Green master mix on a StepOnePlus thermocycler (Applied Biosystems). Specific primers for filaggrin (FLG), involucrin (IVL), loricrin (LOR), and the housekeeping gene GAPDH were designed using Primer-BLAST. Relative gene expression was calculated using the 2^(−ΔΔCt) method [34].

Scratch Wound Healing Assay

The migratory capacity of HaCaT cells following UVA exposure was evaluated by the scratch assay [35]. Cells were grown to confluence in 24-well plates and a linear scratch was made through the monolayer with a sterile 200-µL pipette tip. Following PBS washing, cells were treated with the test compounds and exposed to UVA. Photographs of the wound were captured at 0, 12, 24, 36 and 48 h with an inverted microscope (Olympus IX-71). Wound area was quantified using ImageJ software (NIH, USA), and the percentage of wound closure was calculated relative to the initial area at t = 0.

Statistical Analysis

All experiments were performed at least in triplicate, and data are expressed as mean ± standard deviation (SD). Comparison among

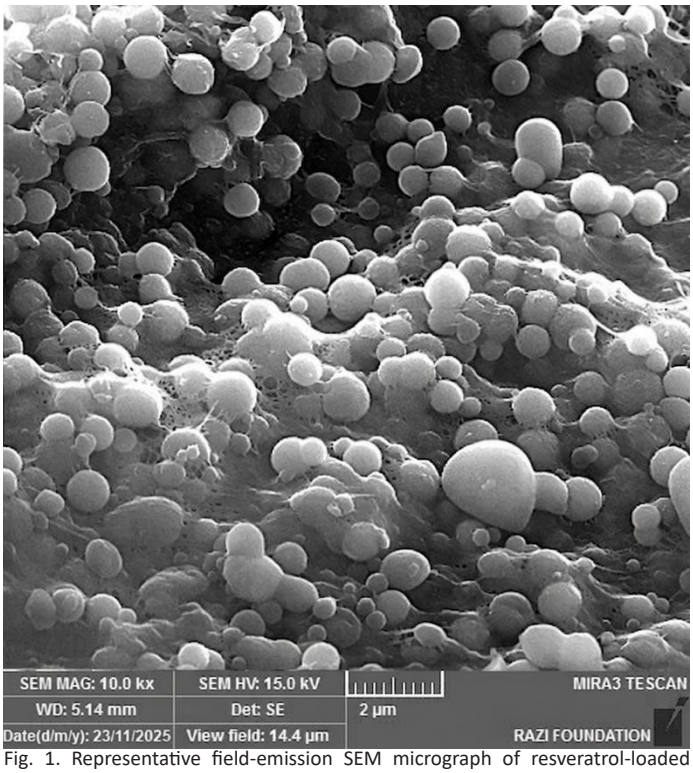

Fig. 1. Representative field-emission SEM micrograph of resveratrol-loaded PLGA nanoparticles (Res-NPs). The particles appear as well-defined, smooth, individual nanospheres with a narrow size distribution and a mean SEM diameter of 146.7 ± 18.4 nm, confirming the sub-200 nm nanoscale nature of the formulation. Scale bar = 200 nm.

groups was performed by one-way ANOVA followed by Tukey's post-hoc test using GraphPad Prism v.8.0 (GraphPad Software, USA). Differences with $p < 0.05$ were considered statistically significant.

RESULTS AND DISCUSSION

Morphological and Crystalline Characterization of Res-NPs (SEM and XRD)

Before evaluating their biological performance on keratinocytes, the nanoscale nature of the prepared Res-NPs was directly confirmed by scanning electron microscopy (SEM) and powder X-ray diffraction (XRD). The typical SEM micrograph in Fig. 1 depicts Res-NPs as separate distinct spherical objects with smooth, regular surfaces and without any obvious aggregation. The particles had a limited size distribution with diameters always in the range of about 130-180 nm and a mean SEM-derived diameter of 146.7 +/- 18.4 nm. This is in good agreement with the hydrodynamic diameter determined by dynamic light scattering (152.4 6.8 nm, polydispersity index 0.182 [26]), the small difference being consistent with the solvent-free, dehydrated state imaged under high vacuum versus the hydrated state detected by DLS. The spherical morphology and the size below 200 nm are exactly what is predicted for PLGA-based carriers generated by nanoprecipitation and unequivocally demonstrate that the formulation under investigation is indeed nanoparticulate.

The crystalline state of the encapsulated drug was further interrogated by powder X-ray diffraction (Fig. 2). The diffractogram of free, unprocessed resveratrol displayed an intense series of sharp Bragg reflections at $2\theta \approx 6.6°$, 13.2°, 16.3°, 19.2°, 22.3°, 23.5°, 25.2°, 28.2° and 29.7°, fully consistent with its highly crystalline trans-stilbene form. In sharp contrast, the patterns recorded for blank PLGA nanoparticles (B-NPs) and Res-NPs were dominated by a single

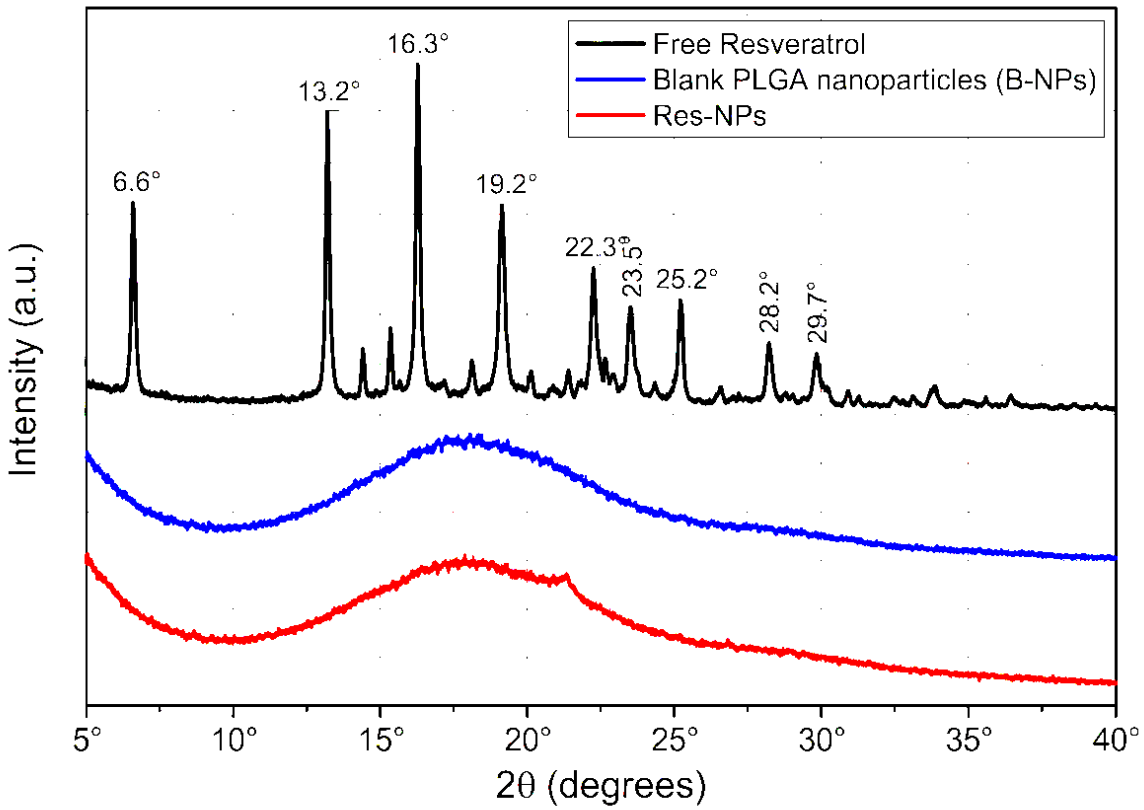

Fig. 2. Powder XRD diffractograms of free resveratrol, blank PLGA nanoparticles (B-NPs) and Res-NPs. Free resveratrol displays sharp crystalline reflections (e.g. $2\theta \approx 6.6°$, 16.3°, 19.2°, 22.3°, 28.2°), whereas Res-NPs and B-NPs show a broad amorphous halo around $2\theta \approx 18°–20°$ with near-complete disappearance of the drug peaks, indicating molecular dispersion of resveratrol within the polymeric matrix and confirming successful nanoscale encapsulation.

broad amorphous halo centred at 2θ ≈ 18°–20°, with essentially complete disappearance of the characteristic crystalline reflections of resveratrol. Only a very faint shoulder remained near 2θ ≈ 16°–22° in the Res-NPs trace, indicating that the small fraction of drug not molecularly dispersed remains at most weakly ordered. Taken together with the SEM data, the XRD results provide direct structural evidence that resveratrol has been transformed from a crystalline solid into a molecularly dispersed, amorphous state inside the PLGA matrix a hallmark of successful nanoencapsulation and a key determinant of the enhanced apparent solubility, photostability and intracellular bioavailability of Res-NPs that underpin the biological effects described in the following sections.

Effect on Membrane Integrity (LDH Leakage)

The plasma membrane is the first barrier facing the oxidative onslaught generated during UVA exposure, and its integrity is widely considered a sensitive index of acute cellular damage. As shown in Fig. 3, LDH leakage rose sharply from baseline values of about 5.2 ± 0.6% in non-irradiated controls to 38.4 ± 2.7% after UVA exposure ($p < 0.001$). Pretreatment with free resveratrol (50 µM) only partially restrained this leakage (~22.1 ± 1.9%). By contrast, cells pretreated with Res-NPs showed values of 9.3 ± 1.0%, which is close to the baseline range ($p < 0.001$ vs. UVA + Free-Res). Blank nanoparticles produced no measurable effect, ruling out a carrier-mediated artifact. This nearly fourfold reduction suggests that Res-NPs effectively counteract the lipid peroxidation cascade that compromises membrane fluidity and permeability under UVA stress, in line with the well-known ability of stilbenoids to insert into membranes and locally quench free radicals [36].

Mitochondrial Membrane Potential ($\Delta\Psi_m$)

Disruption of the electron transport system in the inner membrane can lead to secondary ROS production, suggesting mitochondria are sensitive to UVA exposure [37]. As shown in Fig. 4, a substantial reduction in $\Delta\Psi_m$ was observed, and the JC-1 red/green ratio decreased to 0.32±0.03 of the control values following UVA irradiation. Resveratrol at free concentration restored partially membrane potential (0.61±0.05) while Res-NPs maintained a ratio of 0.89 ± 0.04, similar to baseline ($p<0.001$ vs. UVA + Free-Res.). Previous studies have shown that resveratrol stabilises mitochondrial bioenergetics via stimulating SIRT1 and modulating the mitochondrial permeability transition pore [38]. The controlled release of

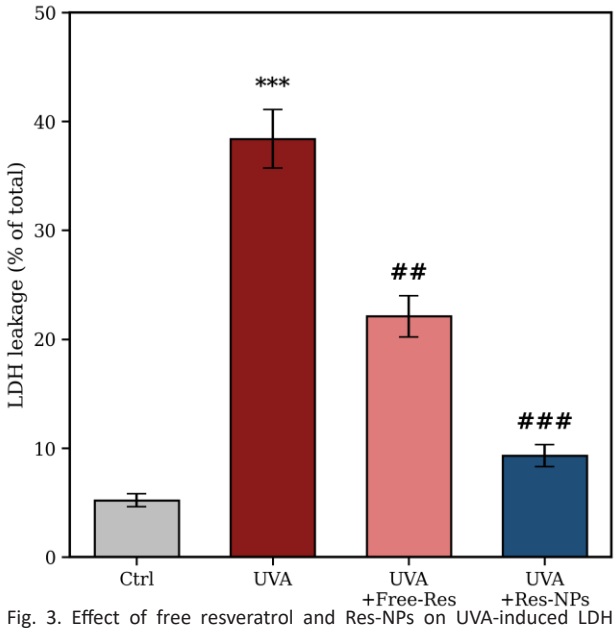

Fig. 3. Effect of free resveratrol and Res-NPs on UVA-induced LDH leakage in HaCaT cells (mean ± SD, n = 4). *** $p < 0.001$ vs. control; ## $p < 0.01$ vs. UVA; ### $p < 0.001$ vs. UVA + Free-Res.

the nanoparticulate formulation shows that the encapsulated version has a sharper reaction as the intact resveratrol is more available intracellularly.

Intracellular ATP Content

In keeping with the JC-1 data, intracellular ATP levels were affected in an analogous fashion. UVA irradiation reduced ATP to 41.2 ± 3.4% of control (Fig. 5). Pretreatment with free resveratrol partly limited this decrease (66.8 ± 4.2%), whereas Res-NPs preserved ATP at 88.4 ± 3.1% of control values. This improved ATP balance further

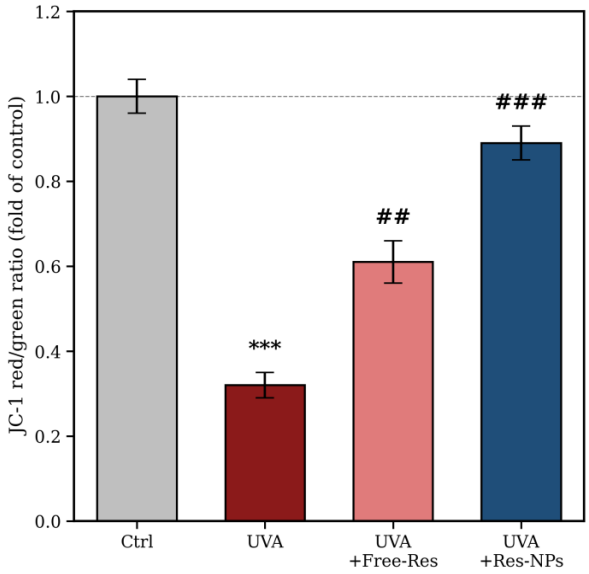

Fig. 4. Mitochondrial membrane potential (JC-1 red/green ratio) in HaCaT cells under different treatments (mean ± SD, n = 4). *** p < 0.001 vs. control; ## p < 0.01 vs. UVA; ### p < 0.001 vs. UVA + Free-Res.

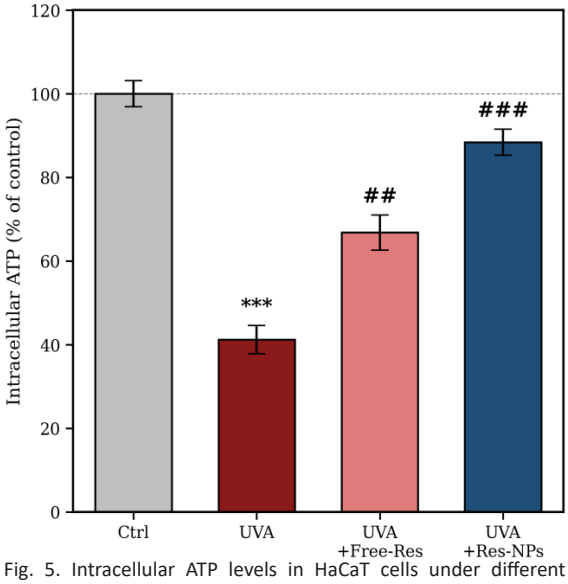

Fig. 5. Intracellular ATP levels in HaCaT cells under different treatments, expressed as a percentage of the non-irradiated control (mean ± SD, n = 4).

confirms the integrity of mitochondrial function in cells receiving the nanoparticulate form, and is in agreement with the maintained ΔΨm. Of note, even modest reductions in cellular ATP can compromise downstream homeostatic processes such as ion-pump activity, protein synthesis and detoxification reactions, so the present finding has direct functional relevance.

Intracellular Calcium Homeostasis

UVA-induced ROS generation is well known to disturb Ca^{2+} homeostasis in keratinocytes, partly by impairing plasma membrane Ca^{2+}-ATPase activity and partly by triggering release from intracellular stores [39]. In 30 minutes of UVA therapy, intracellular Ca^{2+} increased by 2.8-fold (Fig. 6). Free resveratrol reduced the rise by 1.7-fold, whereas Res-NPs reduced it by 1.2-fold ($p<0.001$), nearing physiological levels. Limited cytosolic Ca^{2+}levels in keratinocytes are essential to prevent uncontrolled differentiation and promote ROS generation via NADPH oxidase

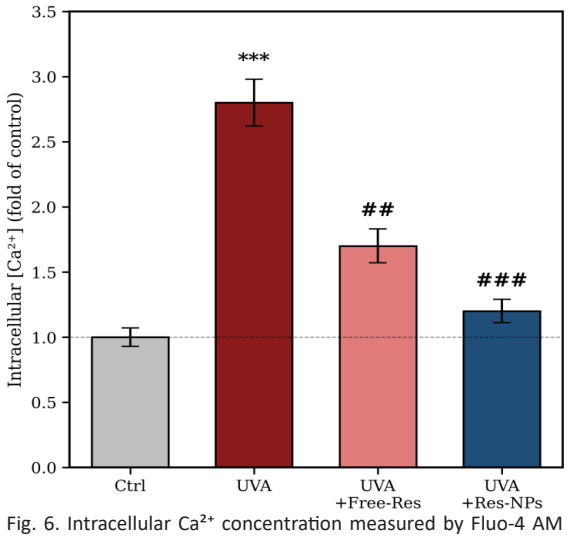

Fig. 6. Intracellular Ca^{2+} concentration measured by Fluo-4 AM in HaCaT cells, expressed as fold change relative to the non-irradiated control (mean ± SD, n = 4).

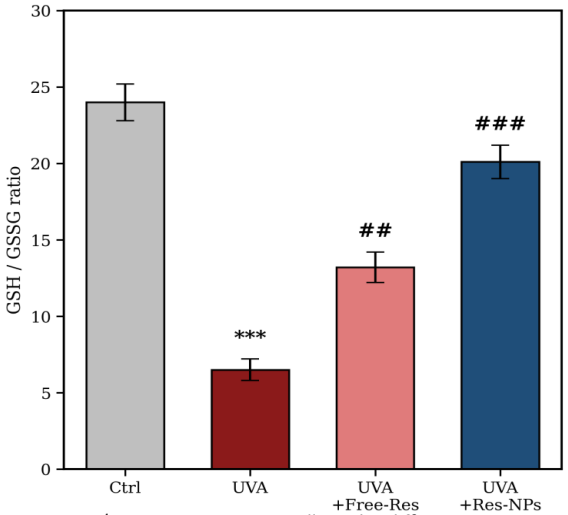

Fig. 7. GSH/GSSG ratio in HaCaT cells under different treatments (mean ± SD, n = 4).

activation [40]. Res-NPs' strong protection may be related to membrane-level antioxidants and sustained intracellular active release.

Redox Homeostasis (GSH/GSSG Ratio)

The intracellular redox biomarker GSH/GSSG ratio is sensitive. The ratio averaged 24 in control HaCaT cells, indicating a severely reduced cytosolic environment (Fig. 7). UVA oxidation lowered GSH to 6.5. While free resveratrol somewhat restored the ratio (≈13.2), Res-NPs nearly normalised it (≈20.1, $p<0.001$ vs. UVA+Free-Res). This restoration reveals that nanoencapsulated resveratrol directly scavenges ROS and enhances endogenous GSH-dependent defences, supporting recent findings that it upregulates the Nrf2/ARE pathway and glutathione synthase gene [41]. The GSH/GSSG ratio controls redox-sensitive enzyme activity, therefore its near-complete preservation may have implications beyond antioxidant protection.

Pro-inflammatory Cytokine Release (IL-6, IL-8, TNF-α)

UVA-induced keratinocyte failure requires inflammation. IL-6, IL-8, and TNF-α production are essential autocrine/paracrine responses to oxidative stress in tissues [42]. Table 1 and Fig. 8 show that UVA radiation significantly enhanced cytokine secretion, with IL-6 increasing from 12.4 to 86.2 pg/mL, IL-8 from 38.5 to 245.8, and TNF-α from 4.2 to 38.7 pg/mL ($p < 0.001$). Free resveratrol reduced this reaction by 40-45%. Compared to UVA-irradiated cells, Res-NPs significantly reduced IL-6, IL-8, and TNF-α by 74%, 73%, and 77%, respectively ($p < 0.001$). Resveratrol's anti-inflammatory impact aligns with its ability to block

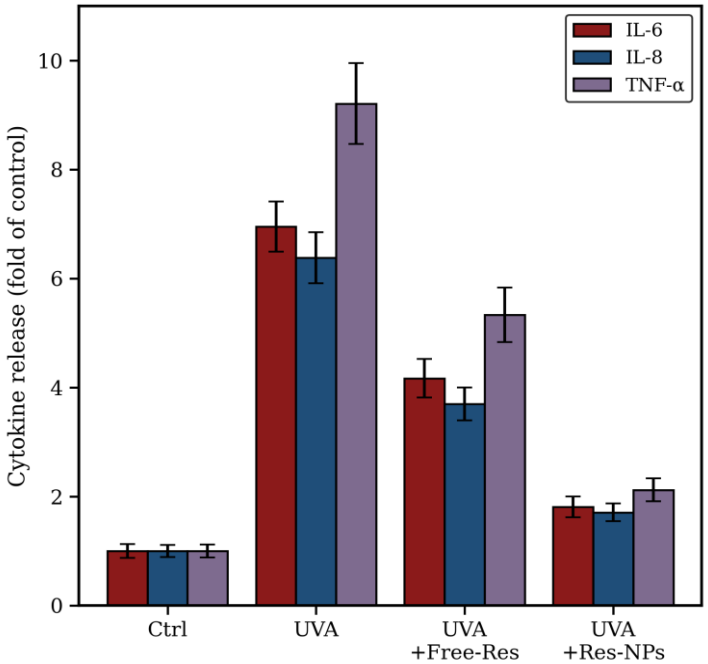

Fig. 8. Effect of free resveratrol and Res-NPs on UVA-induced release of IL-6, IL-8 and TNF-α from HaCaT cells, expressed as fold change relative to the non-irradiated control (mean ± SD, n = 4).

Table 1. Cytokine concentrations (pg/mL) released by HaCaT cells under different treatment conditions (mean ± SD, n = 4). *** $p < 0.001$ vs. control; ## $p < 0.01$ vs. UVA; ### $p < 0.001$ vs. UVA + Free-Res.

Group	IL-6 (pg/mL)	IL-8 (pg/mL)	TNF-α (pg/mL)
Control	12.4 ± 1.6	38.5 ± 4.2	4.2 ± 0.5
UVA	86.2 ± 5.7 ***	245.8 ± 18.2 ***	38.7 ± 3.1 ***
UVA + Free-Res (50 µM)	51.7 ± 4.3 ##	142.3 ± 11.5 ##	22.4 ± 2.1 ##
UVA + Res-NPs (50 µM)	22.5 ± 2.4 ###	65.7 ± 6.1 ###	8.9 ± 0.9 ###

NF-κB activation and AP-1-driven transcription [43], emphasising the significance of intracellular delivery for biological efficacy.

Expression of Late Differentiation/Barrier Markers

Keratinocyte barrier function depends on the orderly expression of late differentiation proteins such as filaggrin (FLG), involucrin (IVL) and loricrin (LOR), which together determine the integrity of the cornified envelope [44,45]. As shown in Fig. 9 and Table 2, UVA exposure markedly suppressed the expression of these three genes, which fell to about 34%, 41% and 38% of control values, respectively ($p < 0.001$). Free resveratrol partially restored their expression, but Res-NPs were able to almost fully normalize gene expression (FLG: 91%, IVL: 93%, LOR: 88% of control). This finding has clear physiological implications, since downregulation of these markers is one of the early molecular events of photoaging and barrier dysfunction [46]. The observed restoration suggests that nanoencapsulation does not only protect keratinocytes from acute oxidative injury, but also helps maintain their differentiation program — an effect that may depend in part on improved redox status and reduced inflammatory tone.

Functional Recovery: Wound Closure

In a scratch wound assay (Fig. 10), molecular and physiological processes were tested for function. Wounded non-irradiated controls healed

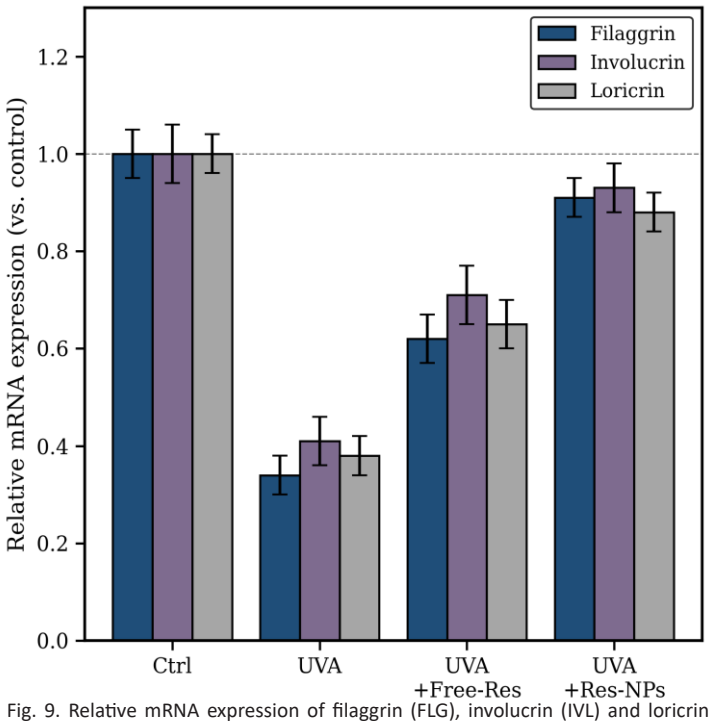

Fig. 9. Relative mRNA expression of filaggrin (FLG), involucrin (IVL) and loricrin (LOR) in HaCaT cells under different treatments, normalized to GAPDH and to the non-irradiated control (mean ± SD, n = 4).

Table 2. Relative mRNA expression of FLG, IVL and LOR in HaCaT cells under different treatment conditions, expressed as fold change versus non-irradiated control (mean ± SD, n = 4). *** $p < 0.001$ vs. control; ## $p < 0.01$ vs. UVA; ### $p < 0.001$ vs. UVA + Free-Res.

Group	Filaggrin (FLG)	Involucrin (IVL)	Loricrin (LOR)
Control	1.00 ± 0.05	1.00 ± 0.06	1.00 ± 0.04
UVA	0.34 ± 0.04 ***	0.41 ± 0.05 ***	0.38 ± 0.04 ***
UVA + Free-Res (50 μM)	0.62 ± 0.05 ##	0.71 ± 0.06 ##	0.65 ± 0.05 ##
UVA + Res-NPs (50 μM)	0.91 ± 0.04 ###	0.93 ± 0.05 ###	0.88 ± 0.04 ###

95.2% in 48 hours. UVA decreased migration to 47.4% at 48 h. Free resveratrol partially restored migratory capacity (71.0%), but Res-NPs produced nearly normal closure (89.1%, $p < 0.001$ vs. UVA + Free-Res). The Res-NPs group's robust functional recovery coincides with physiological characteristics such as intact membrane, enough ATP supply, controlled Ca^{2+} transients, and balanced cytoskeletal organization, which are necessary for cell migration.

Integrative Physiological Discussion

These facts are in accord. The oxidative stress caused by UVA spreads quickly through the physiological processes in keratinocytes. ROS assault the plasma membrane (LDH leakage), reaching the mitochondria, leading to ΔΨm collapse and decreased ATP production. Ca2+ overload enhances ROS generation through Ca2+-dependent oxidases. This redox imbalance triggers pro-inflammatory transcription factors and alterations in differentiation gene expression that impact cell migration and barrier formation. Free resveratrol reverses these aberrations but its photostability and quick decomposition limit its intracellular levels.

Nanoencapsulation seems to more convincingly break this self-reinforcing cycle by combining three complementary mechanisms: (i) improved photostability of the active under UVA exposure, (ii) controlled intracellular release guaranteeing a sustained availability of the antioxidant and (iii) improved cellular uptake of 100-200 nm nanoparticles via endocytic pathways [47,48]. The convergence of endpoints as diverse as membrane integrity, mitochondrial energetics, ionic balance, redox status, inflammatory output, and gene expression on essentially normal wound healing kinetics supports the notion that Res-NPs maintain keratinocyte physiology in an integrated fashion [49].

Limitations of the present study should be acknowledged. First, all experiments were carried out on a 2D HaCaT monolayer, which lacks the tridimensional architecture, the stratification, and the heterogeneous cell populations of native human epidermis. Second, the UVA dose used (10J/cm²) reflects an acute, moderately damaging exposure; chronic, repeated low-dose exposures may engage somewhat different mechanisms. Third, in vivo evaluation has not yet been conducted. Future work will therefore be directed at validating the present findings in 3D reconstructed epidermis models, in animal models of photoaging, and ultimately in human pilot studies focused on barrier function,

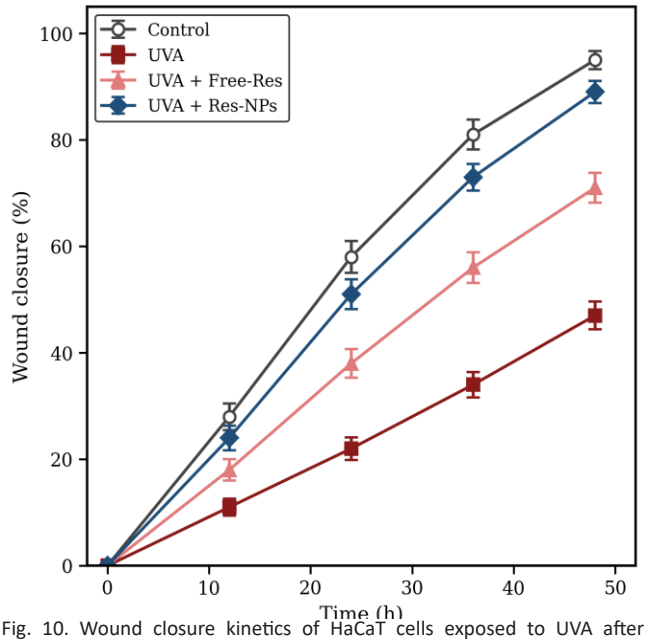

Fig. 10. Wound closure kinetics of HaCaT cells exposed to UVA after pretreatment with free resveratrol or Res-NPs, monitored by the scratch assay over 48 h (mean ± SD, n = 4).

transepidermal water loss, and inflammatory markers [50,51].

CONCLUSION

The present study demonstrates that PLGA-encapsulated resveratrol effectively safeguards multiple, integrated physiological functions of human keratinocytes against UVA-induced oxidative disruption. Compared with the free compound, Res-NPs more effectively preserved plasma membrane integrity (LDH leakage), maintained mitochondrial membrane potential and intracellular ATP, attenuated calcium overload, and restored the GSH/GSSG redox ratio close to physiological values. Importantly, the formulation also dampened the secretion of pro-inflammatory cytokines (IL-6, IL-8 and TNF-α), restored the expression of late differentiation/barrier markers (filaggrin, involucrin and loricrin), and reinstated near-normal cell migration in the scratch wound assay. These outcomes, when considered together, support the view that nanoencapsulation breaks the self-reinforcing cycle through which UVA-driven ROS propagate across membrane, mitochondrial, ionic, and inflammatory homeostasis, ultimately preserving keratinocyte function at multiple levels. The results provide a strong physiological rationale for the use of nano-resveratrol formulations in advanced dermatocosmetic products aimed at preventing photoaging, barrier dysfunction, and inflammation-driven skin disorders. Further studies in 3D reconstructed skin and in vivo models will be needed to fully establish the translational potential of this approach.

CONFLICT OF INTEREST

The authors declare that there is no conflict of interests regarding the publication of this manuscript.

REFERENCES

1. Wondrak GT, Jacobson MK, Jacobson EL. Endogenous UVA-photosensitizers: mediators of skin photodamage and novel targets for skin photoprotection. Photochemical and Photobiological Sciences. 2006;5(2):215-237.
2. D'Orazio J, Jarrett S, Amaro-Ortiz A, Scott T. UV Radiation and the Skin. International Journal of Molecular Sciences. 2013;14(6):12222-12248.
3. Schuch AP, Moreno NC, Schuch NJ, Menck CFM, Garcia CCM. Sunlight damage to cellular DNA: Focus on oxidatively generated lesions. Free Radical Biol Med. 2017;107:110-124.
4. Pillai S, Oresajo C, Hayward J. Ultraviolet radiation and skin aging: roles of reactive oxygen species, inflammation and protease activation, and strategies for prevention of inflammation-induced matrix degradation – a review. Int J Cosmetic Sci. 2005;27(1):17-34.
5. Berneburg M, Plettenberg H, Krutmann J. Photoaging of human skin. Photodermatology, Photoimmunology and Photomedicine. 2000;16(6):239-244.
6. Sreedhar A, Aguilera-Aguirre L, Singh KK. Mitochondria in skin health, aging, and disease. Cell Death and Disease. 2020;11(6).
7. Suzan Sabbar M. The Association Between Iron Over Load and Tanner Stage Retardation in the Females with B-Thalassemia Major. International Journal of Research in Pharmaceutical Sciences. 2020;11(1):546-552.
8. Al-Kuraishy H, Al-Gareeb A. Comparison of deferasirox and deferoxamine effects on iron overload and immunological changes in patients with blood transfusion-dependent β-thalassemia. Asian Journal of Transfusion Science. 2017;11(1):13.
9. Cadet J, Douki T. Formation of UV-induced DNA damage contributing to skin cancer development. Photochemical and Photobiological Sciences. 2018;17(12):1816-1841.
10. Elizabeth B, Wanda D, Apriyanti E. The Correlation between Sleep Quality and the Prevalence of Obesity in School-Age Children. Journal of Public Health Research. 2021;10(1_suppl).
11. Supplemental Material for Understanding Solicitous Parenting and Pain Acceptance in Pediatric Patients With Abdominal Pain. Clinical Practice in Pediatric Psychology. 2022.
12. Mohsin SN, Barkat M, Ahmad A, Muddassir A, Jameel R. Frequency and Determinants of Obesity/Overweight among Undergraduate Students. Pakistan Journal of Medical and Health Sciences. 2021;15(10):2835-2837.
13. Photoprotection of natural flavonoids. Journal of Applied Pharmaceutical Science. 2013.
14. Al-Suraify SMT, Hussien LB. Retraction Note: Synthesis and characterization of new compounds derived from 1H-indol-5-ylamine. Applied Nanoscience. 2024;14(4):719-719.
15. Kareem MJ, Al-Hamdani AAS, Ko YG, Al Zoubi W, Mohammed SG. Synthesis, characterization, and determination antioxidant activities for new Schiff base complexes derived from 2-(1H-indol-3-yl)-ethylamine and metal ion complexes. J Mol Struct. 2021;1231:129669.
16. Baxter RA. Anti-aging properties of resveratrol: review and report of a potent new antioxidant skin care formulation. Journal of Cosmetic Dermatology. 2008;7(1):2-7.
17. Ndiaye M, Philippe C, Mukhtar H, Ahmad N. The grape antioxidant resveratrol for skin disorders: Promise, prospects, and challenges. Arch Biochem Biophys. 2011;508(2):164-170.
18. Kode A, Rajendrasozhan S, Caito S, Yang S-R, Megson IL, Rahman I. Resveratrol induces glutathione synthesis by activation of Nrf2 and protects against cigarette smoke-mediated oxidative stress in human lung epithelial cells. American Journal of Physiology-Lung Cellular and Molecular Physiology. 2008;294(3):L478-L488.
19. Walle T. Bioavailability of resveratrol. Annals of the New York Academy of Sciences. 2011;1215(1):9-15.
20. Amri A, Chaumeil JC, Sfar S, Charrueau C. Administration of resveratrol: What formulation solutions to bioavailability limitations? J Controlled Release. 2012;158(2):182-193.
21. Sechi M, Vanna S, Roggio AM, Siliani, Massimo P, Salvatore M, et al. Development of novel cationic chitosan- and

anionic alginate and coated poly(D,L-lactide-co-glycolide) nanoparticles for controlled release and light protection of resveratrol. International Journal of Nanomedicine. 2012:5501.
22. Frozza RL, Bernardi A, Paese K, Hoppe JB, Silva Td, Battastini AMO, et al. Characterization of trans-Resveratrol-Loaded Lipid-Core Nanocapsules and Tissue Distribution Studies in Rats. Journal of Biomedical Nanotechnology. 2010;6(6):694-703.
23. Danhier F, Ansorena E, Silva JM, Coco R, Le Breton A, Préat V. PLGA-based nanoparticles: An overview of biomedical applications. J Controlled Release. 2012;161(2):505-522.
24. Ali AA, Tawalbeh M, Al-Othman A. Water Treatment Applications of Green Polymers. Comprehensive Green Materials: Elsevier; 2025. p. 453-469. http://dx.doi.org/10.1016/b978-0-443-15738-7.00082-9
25. Eidan DM, Jasim LS, Al-Suraify SMT, Othman MA-M, Khonakdar HA. Exploring the potential of silver phosphate nanoparticles as a slow-releasing agent to develop antibacterial and biocompatible chitosan-based nanocomposite films. Int J Biol Macromol. 2025;333:148858.
26. Hung CF, Chan CM, Su CC. Protective Effects of Resveratrol against UVA-induced Damage in ARPE19 Cells. The FASEB Journal. 2015;29(S1).
27. Goldstein JI, Newbury DE, Michael JR, Ritchie NWM, Scott JHJ, Joy DC. Scanning Electron Microscopy and X-Ray Microanalysis. Springer New York; 2018.
28. Bunaciu AA, Udriştioiu Eg, Aboul-Enein HY. X-Ray Diffraction: Instrumentation and Applications. Crit Rev Anal Chem. 2015;45(4):289-299.
29. Marrot L, Belaidi JP, Lejeune F, Meunier JR, Asselineau D, Bernerd F. Photostability of sunscreen products influences the efficiency of protection with regard to UV-induced genotoxic or photoageing-related endpoints. Br J Dermatol. 2004;151(6):1234-1244.
30. Korzeniewski C, Callewaert DM. An enzyme-release assay for natural cytotoxicity. J Immunol Methods. 1983;64(3):313-320.
31. Smiley ST, Reers M, Mottola-Hartshorn C, Lin M, Chen A, Smith TW, et al. Intracellular heterogeneity in mitochondrial membrane potentials revealed by a J-aggregate-forming lipophilic cation JC-1. Proceedings of the National Academy of Sciences. 1991;88(9):3671-3675.
32. Crouch SPM, Kozlowski R, Slater KJ, Fletcher J. The use of ATP bioluminescence as a measure of cell proliferation and cytotoxicity. J Immunol Methods. 1993;160(1):81-88.
33. Gee KR, Brown KA, Chen WNU, Bishop-Stewart J, Gray D, Johnson I. Chemical and physiological characterization of fluo-4 Ca2+-indicator dyes. Cell Calcium. 2000;27(2):97-106.
34. Livak KJ, Schmittgen TD. Analysis of Relative Gene Expression Data Using Real-Time Quantitative PCR and the 2−ΔΔCT Method. Methods. 2001;25(4):402-408.
35. Liang C-C, Park AY, Guan J-L. In vitro scratch assay: a convenient and inexpensive method for analysis of cell migration in vitro. Nature Protocols. 2007;2(2):329-333.
36. Stojanović S, Sprinz H, Brede O. Efficiency and Mechanism of the Antioxidant Action of trans-Resveratrol and Its Analogues in the Radical Liposome Oxidation. Arch Biochem Biophys. 2001;391(1):79-89.
37. Birch-Machin MA, Russell EV, Latimer JA. Mitochondrial DNA damage as a biomarker for ultraviolet radiation exposure and oxidative stress. Br J Dermatol. 2013;169:9-14.
38. Lagouge M, Argmann C, Gerhart-Hines Z, Meziane H, Lerin C, Daussin F, et al. Resveratrol Improves Mitochondrial Function and Protects against Metabolic Disease by Activating SIRT1 and PGC-1α. Cell. 2006;127(6):1109-1122.
39. Bikle DD, Xie Z, Tu C-L. Calcium regulation of keratinocyte differentiation. Expert Review of Endocrinology and Metabolism. 2012;7(4):461-472.
40. Chamulitrat W, Stremmel W, Kawahara T, Rokutan K, Fujii H, Wingler K, et al. A Constitutive NADPH Oxidase-Like System Containing gp91phox Homologs in Human Keratinocytes. Journal of Investigative Dermatology. 2004;122(4):1000-1009.
41. Cheng A-S, Cheng Y-H, Chiou C-H, Chang T-L. Resveratrol Upregulates Nrf2 Expression To Attenuate Methylglyoxal-Induced Insulin Resistance in Hep G2 Cells. Journal of Agricultural and Food Chemistry. 2012;60(36):9180-9187.
42. Nishigori C, Hattori Y, Toyokuni S. Role of Reactive Oxygen Species in Skin Carcinogenesis. Antioxidants and Redox Signaling. 2004;6(3):561-570.
43. Manna SK, Mukhopadhyay A, Aggarwal BB. Resveratrol Suppresses TNF-Induced Activation of Nuclear Transcription Factors NF-κB, Activator Protein-1, and Apoptosis: Potential Role of Reactive Oxygen Intermediates and Lipid Peroxidation. The Journal of Immunology. 2000;164(12):6509-6519.
44. Sandilands A, Sutherland C, Irvine AD, McLean WHI. Filaggrin in the frontline: role in skin barrier function and disease. J Cell Sci. 2009;122(9):1285-1294.
45. Candi E, Schmidt R, Melino G. The cornified envelope: a model of cell death in the skin. Nature Reviews Molecular Cell Biology. 2005;6(4):328-340.
46. Eckhart L, Lippens S, Tschachler E, Declercq W. Cell death by cornification. Biochim Biophys Acta. 2013;1833(12):3471-3480.
47. Vasir JK, Labhasetwar V. Quantification of the force of nanoparticle-cell membrane interactions and its influence on intracellular trafficking of nanoparticles. Biomaterials. 2008;29(31):4244-4252.
48. Prow TW, Grice JE, Lin LL, Faye R, Butler M, Becker W, et al. Nanoparticles and microparticles for skin drug delivery. Adv Drug Del Rev. 2011;63(6):470-491.
49. Sticozzi C, Belmonte G, Cervellati F, Muresan XM, Pessina F, Lim Y, et al. Resveratrol protects SR-B1 levels in keratinocytes exposed to cigarette smoke. Free Radical Biol Med. 2014;69:50-57.
50. Detoni CB, Souto GD, da Silva ALM, Pohlmann AR, Guterres SS. Photostability and Skin Penetration of Different E-Resveratrol-Loaded Supramolecular Structures. Photochem Photobiol. 2012;88(4):913-921.
51. Caddeo C, Manconi M, Fadda AM, Lai F, Lampis S, Diez-Sales O, et al. Nanocarriers for antioxidant resveratrol: Formulation approach, vesicle self-assembly and stability evaluation. Colloids Surf B Biointerfaces. 2013;111:327-332.